Enhanced Magnetic Sensitivity with Non-Gaussian Quantum Fluctuations

Chayma Bouazza, Davide Dreon, Alexandre A. Evrard, Vasiliy Makhalov, Thomas Chalopin, Leonid A Sidorenkov, Jean Dalibard, Raphael Lopes, Sylvain Nascimbene

Enhanced Magnetic Sensitivity with Non-Gaussian Quantum Fluctuations

Alexandre Evrard, Vasiliy Makhalov, Thomas Chalopin, Leonid A. Sidorenkov,*
Jean Dalibard, Raphael Lopes, and Sylvain Nascimbene†
Laboratoire Kastler Brossel, Collège de France, CNRS, ENS-PSL University, Sorbonne Université, 11 Place Marcelin Berthelot, 75005 Paris, France

(Received 18 January 2019; published 1 May 2019)

The precision of a quantum sensor can overcome its classical counterpart when its constituents are entangled. In Gaussian squeezed states, quantum correlations lead to a reduction of the quantum projection noise below the shot noise limit. However, the most sensitive states involve complex non-Gaussian quantum fluctuations, making the required measurement protocol challenging. Here we measure the sensitivity of nonclassical states of the electronic spin $J = 8$ of dysprosium atoms, created using light-induced nonlinear spin coupling. Magnetic sublevel resolution enables us to reach the optimal sensitivity of non-Gaussian (oversqueezed) states, well above the capability of squeezed states and about half the Heisenberg limit.

DOI: 10.1103/PhysRevLett.122.173601

The measurement of a physical quantity is fundamentally limited in precision by the quantum nature of the measurement apparatus, via the Heisenberg uncertainty principle [1,2]. Similarly, to the mere averaging of N independent measurements, a measurement device made of N independent quantum probes allows reducing the measurement uncertainty by a factor $\sqrt{N}$ compared to a single realization, leading to the standard quantum limit of precision (SQL). Conversely, a set of correlated quantum probes may reach a better sensitivity [3,4], ultimately up to the Heisenberg limit—a measurement uncertainty reduced by a factor N [5]. However, reaching this precision limit with large-size quantum systems remains challenging, because it requires manipulating highly entangled quantum states, whose increased measurement sensitivity comes together with a higher fragility to environmental perturbations [6].

A quantum sensitivity enhancement has been demonstrated in various experimental settings, including photonic systems [7–9], trapped ions [10–14], Rydberg atoms [15], thermal atomic gases [16–21], or Bose-Einstein condensates [22–31]. In squeezed quantum states described by Gaussian statistics, fluctuations of the mean response of the N probes are reduced below the shot noise limit, thus increasing the measurement precision [3]. In the most common squeezing protocols, the measurement uncertainty is decreased by a factor $N^{2/3}$ intermediate between the SQL and the Heisenberg limit [32,33]. The precision can be further improved using states with non-Gaussian quantum fluctuations, characterized by high-order correlations between all probes [34]. Quantum sensing with such non-Gaussian states has been demonstrated in Refs. [14,30]; yet, the reported spectroscopic enhancement values remain limited, because reaching optimal sensitivity typically requires single-particle resolution [35,36] or nonlinear detection [37–40].

In this Letter, we use ultracold samples of atomic dysprosium to study the magnetic-field sensitivity of Gaussian and non-Gaussian quantum spin states, encoded for each atom in its electronic spin of size $J = 8$—equivalent to a set of precisely $N = 2J = 16$ elementary spin-1/2 particles [41]. We use spin-dependent light shifts to induce nonlinear dynamics described by the one-axis twisting Hamiltonian $\hat{H} = \hbar\chi\hat{J}_x^2$ [32]. These dynamics generate Gaussian squeezed states at short times, before the stretching of spin distribution leads to non-Gaussian "oversqueezed" states. Single magnetic sublevel resolution gives us access to the magnetic sensitivity hidden in non-Gaussian quantum fluctuations, yielding a spectroscopic enhancement of 8.6(6) compared to the SQL, consistent with the maximum sensitivity $J + 1/2$ expected for oversqueezed states and about half the Heisenberg limit. We stress that our method is not based on correlations between different atoms but rather exploits the spin degree of freedom of individual atoms. A clear asset for our procedure robustness is the absence of effective constituents number fluctuations $N = 2J$.

The experimental protocol is pictured in Fig. 1. We first prepare a gas of $1.0(2) \times 10^5$ atoms of ^{162}Dy at a temperature $T = 1.1(2)\ \mu$K, using standard cooling techniques [42]. The atoms are initially spin polarized in the absolute ground state $|m = -J>_z$, under a quantization field $\mathbf{B} = B\hat{\mathbf{z}}$, with $B = 60.6(3)$ mG. We shine on the atoms an off-resonant laser beam inducing spin-dependent light shifts thanks to the proximity to the narrow 626-nm optical transition (natural linewidth $\Gamma \simeq 0.85\ \mu\text{s}^{-1}$). For a linear light polarization along $\hat{\mathbf{x}}$, the light shift reduces (up to a

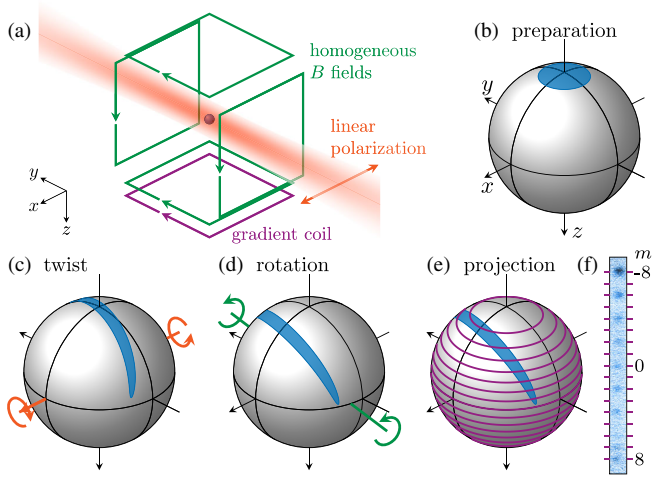

FIG. 1. (a) Scheme of the experimental setup. Starting with a coherent state of the electronic spin of dysprosium atoms aligned with the south pole (b), we induce nonlinear dynamics using an off-resonant laser beam (c). We then perform a spin rotation (d) followed by a projective measurement along z using a magnetic field gradient (e). A typical absorption image is shown in (f).

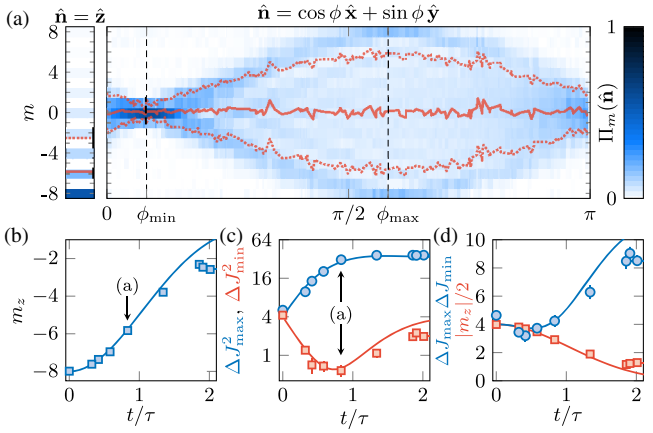

FIG. 2. (a) Projection probabilities $\Pi_m(\hat{\mathbf{n}})$ along $\hat{\mathbf{n}} = \hat{\mathbf{z}}$ and $\hat{\mathbf{n}} \perp \hat{\mathbf{z}}$, for an interaction time $t = 0.83(1)\tau$, with $\tau = (\sqrt{2J}\chi)^{-1}$. The solid (dotted) red line indicates the magnetization $m_{\hat{\mathbf{n}}}$ (values of $m_{\hat{\mathbf{n}}} \pm \Delta J_{\hat{\mathbf{n}}}$). (b) Magnetization m_z as a function of the interaction time t. (c) Maximum and minimum spin projection variances $\Delta J^2_{\max}$ and $\Delta J^2_{\min}$ (blue dots and red squares, respectively). (d) Comparison between the uncertainty product $\Delta J_{\max}\Delta J_{\min}$ and the half mean spin length $|m_z|/2$. The solid lines in (b)–(d) correspond to the one-axis twisting model predictions. In all figures of this Letter error bars represent the 1-σ statistical uncertainty determined using a bootstrap sampling method.

constant) to a coupling $\hbar\chi\hat{J}_x^2$, where the rate χ is proportional to the light intensity (in the range $\chi \sim 1$–$10\ \mu s^{-1}$) [43,44]. Over the typical pulse duration, $t \sim 100$ ns, the Larmor rotation induced by the quantization magnetic field is $\sim 3°$ only, and we neglect it hereafter. We thus expect the dynamics to be well described solely by the one-axis twisting Hamiltonian [see Fig. 1(c)]. After the nonlinear spin dynamics, we apply time-dependent magnetic fields to rotate the spin along arbitrary directions [see Fig. 1(d)]. We finally perform a projective measurement along z using a magnetic field gradient that spatially separates the $|m>_z$ magnetic sublevels after a free expansion of 2.45 ms [see Figs. 1(e) and 1(f)]. Combining rotation and projective measurement gives us access to the projection probabilities $\Pi_m(\hat{\mathbf{n}})$ $(-J \le m \le J)$ along any direction $\hat{\mathbf{n}}$ [45].

We first characterize the produced spin states by measuring their first and second spin moments. We expect from the symmetry of the one-axis twisting Hamiltonian that the mean spin $\mathbf{m} \equiv \langle \hat{\mathbf{J}} \rangle$ remains oriented along z. An example of populations $\Pi_m(\hat{\mathbf{z}})$ is shown in Fig. 2(a), from which we extract the magnetization m_z. We find that the magnetization decreases with time in absolute value as expected from the one-axis twisting model [see Fig. 2(b)]. We also plot in Fig. 2(a) projection probabilities measured along directions $\hat{\mathbf{n}} \perp \hat{\mathbf{z}}$, from which we extract the minimum (maximum) uncertainty $\Delta J_{\min}$ ($\Delta J_{\max}$), for a projection direction $\hat{\mathbf{n}}_{\min}$ ($\hat{\mathbf{n}}_{\max}$) of azimutal angle $\phi_{\min}$ ($\phi_{\max}$, respectively).

For $t = 0$, the spin is polarized in $|-J\rangle_z$, corresponding to a coherent spin state. This state constitutes the best representation of a classical state magnetized along $-\hat{\mathbf{z}}$, with zero magnetization along x and y, and projection uncertainties $\Delta J_x/J = \Delta J_y/J = 1/\sqrt{2J}$ taking the minimum value allowed for an isotropic distribution in the xy plane [48]. For this state, we find that for all directions $\hat{\mathbf{n}} \perp \hat{\mathbf{z}}$ the population distributions remain identical, and the projection variance $\Delta J^2_{\hat{\mathbf{n}}} = 4.3(2)$, as expected [48]. For $t > 0$, we measure a squeezing of the minimum projection uncertainty down to $\Delta J^2_{\min} = 0.6(1)$, i.e., about seven times smaller than the coherent state value [see Fig. 2(c)]. The maximum spin quadrature $\Delta J^2_{\max}$ increases with t up to a value $\simeq 37(1)$. This behavior is consistent with a semiclassical picture of spin "diffusion" over the entire yz meridian, leading to steady asymptotic values $\Delta J^2_{\min} = \Delta J^2_x = J/2$ and $\Delta J^2_{\max} = \Delta J^2_y = \Delta J^2_z = J(J+\frac{1}{2})/2 = 34$. We find this dynamics to occur on the timescale of the diffusion time $\tau \equiv (\sqrt{2J}\chi)^{-1}$ expected within the one-axis twisting model [32]. We also use these measurements to quantify the Gaussian character of quantum fluctuations, characterized by a saturation of the Heisenberg uncertainty relation $\Delta J_{\max}\Delta J_{\min} \ge |m_z|/2$ [49]. As shown in Fig. 2(d), we find that this inequality is saturated for $t < 0.5\tau$, while non-Gaussian states occur for longer times.

We now discuss magnetic field sensing, i.e., the estimation of small rotation angles ν around an axis $\hat{\mathbf{b}}$. In the most basic scheme, one estimates the angle ν from a measurement of the mean spin projection, giving access to the magnetization m_z up to the projection noise ΔJ_z. The single-shot uncertainty on the estimation of ν then reads $\Delta\nu = \Delta J_z/|dm_z/d\nu|$ [1]. For a set of $N = 2J$ uncorrelated spins 1/2, optimal sensitivity $\Delta\nu_{\mathrm{SQL}} = 1/\sqrt{2J}$ is expected

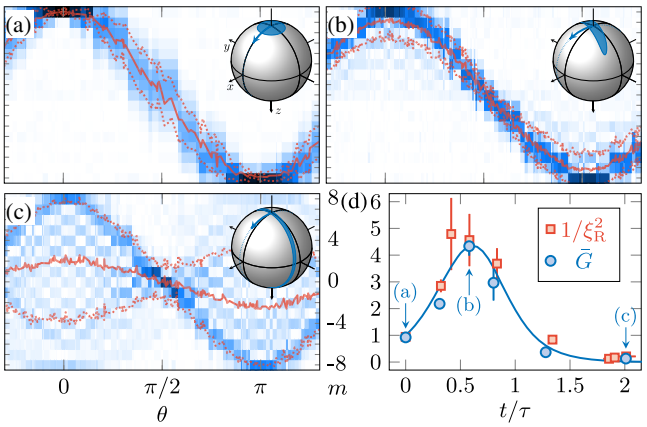

FIG. 3. (a),(b) Evolution of the projection probabilities Π_m upon a Larmor rotation of angle θ around the direction $\hat{\mathbf{n}}_{\max}$ of maximum sensitivity, for a coherent state (a), a squeezed state (b) [interaction time $t = 0.58(2)\tau$] and an oversqueezed state [c, $t = 2.01(1)\tau$]. The solid (dotted) red line corresponds to the magnetization m_z (values of $m_z \pm \Delta J_z$) computed from the Π_m values. (d) Usual metrological gain $\bar{G}$ and value of $1/\xi_R^2$ deduced from the Figs. 2(b) and 2(c) data as a function of the interaction time t. The solid line corresponds to the one-axis twisting model prediction.

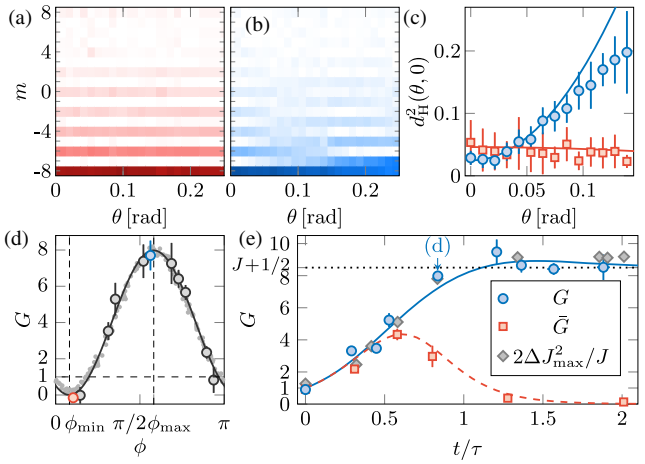

FIG. 4. (a),(b) Projection probabilities Π_m measured for small rotation angles θ around $\hat{\mathbf{b}} = \cos\phi\hat{\mathbf{x}} + \sin\phi\hat{\mathbf{y}}$, with $\phi = 0.10(2)\pi \simeq \phi_{\min}$ and $0.56(2)\pi \simeq \phi_{\max}$, respectively, for an interaction time $t = 0.835(5)\tau$. Each probability is the average of three independent experiments. (c) Hellinger distances $d_H^2(\theta, 0)$ deduced from (a),(b), together with a quadratic fit of the small-θ data. (d) Metrological gain G deduced from the curvature of the Hellinger distance as a function of the azimutal angle ϕ (gray circles). The black line is a sine fit of the data. Gray dots correspond to the upper bound $2\Delta J_{\hat{\mathbf{b}}}^2/J$ extracted from the Fig. 2(a) data. (e) Measured metrological gain G (blue dots) as a function of the interaction time t. The gray diamonds correspond to the upper bound $2\Delta J_{\max}^2/J$ [from Fig. 2(c)], and the red squares are the $\bar{G}$ values from Fig. 3(d). The solid blue and dashed red lines correspond to the gains G and $\bar{G}$ expected from the one-axis twisting model.

when all probes are aligned together, corresponding to a coherent spin state [48], and for a rotation axis $\hat{\mathbf{b}} \perp \mathbf{m}$. To check this behavior, we measure the precession of the coherent state $|m = -J>_z$ around a direction $\hat{\mathbf{b}} \perp \hat{\mathbf{z}}$, parametrized by the angle θ [see Fig. 3(a)]. We estimate the sensitivity of the state obtained after a rotation $\theta_0 = \pi/2$ by evaluating the slope $dm_z/d\nu = -8.01(4)$ at the vicinity of θ_0. We extract, at this angle, a value of $\Delta J_z^2 = 4.3(1)$, leading to $\Delta\nu = 1.04(3)\Delta\nu_{\mathrm{SQL}}$, which validates our procedure.

We extend this measurement to the states produced after nonlinear dynamics. We observe a decrease of the magnetization oscillation amplitude corresponding to the reduction of the mean spin length [see Figs. 3(b) and 3(c)]. The best magnetic sensitivity is achieved for a rotation axis $\hat{\mathbf{b}}$ coinciding with the direction $\hat{\mathbf{n}}_{\max}$ of maximal spin projection variance $\Delta J_{\max}$ and around $\theta = \pi/2$. We quantify the increase of sensitivity with respect to the SQL by the metrological gain $\bar{G} \equiv (\Delta\nu_{\mathrm{SQL}}/\Delta\nu)^2$ [50]. For durations $0 < t < \tau$ we observe a quantum enhancement $\bar{G} > 1$, with a maximum gain $\bar{G} = 4.3(4)$ reached for $t = 0.58(2)\tau$. As shown in Fig. 3(d), our data are in good agreement with the one-axis twisting model predictions [32]. We expect the sensitivity to be related to the minimum spin projection variance $\Delta J_{\min}$, as $\bar{G} = 1/\xi_R^2$, where we introduce the so-called spin squeezing parameter $\xi_R \equiv \sqrt{2J}\Delta J_{\min}/|m_z|$ [4]. We verify this relation in Fig. 3(d), where the ξ_R values are computed from the measured m_z and $\Delta J_{\min}$ data. For $t > \tau$, we observe that the gain $\bar{G}$ drops below unity, as expected from the mean spin length reduction.

To go beyond this "usual" metrological gain $\bar{G}$, we now exploit a key feature of our setup, i.e., the ability to resolve individual sublevels. This allows us to unveil small-scale structures in the measured projection probabilities $\Pi_m(\theta)$ that rapidly vary with θ, suggesting hidden phase sensitivity in higher-order moments of the probability distribution, even when $\bar{G} < 1$. In order to quantify this θ dependence, we introduce the Hellinger distance between probability distributions $d_H^2(\theta, \theta') \equiv \frac{1}{2}\sum_m[\sqrt{\Pi_m(\theta)} - \sqrt{\Pi_m(\theta')}]^2$. The phase sensitivity, expressed in terms of metrological gain, is then related to the curvature of the Hellinger distance as [30,51]

$$G(\theta) = \frac{2}{J}\frac{\partial^2 d_H^2(\theta, \theta+\nu)}{\partial\nu^2}\bigg|_{\nu=0}. \quad (1)$$

This gain coincides with the usual gain $\bar{G}$ for states with Gaussian quantum fluctuations.

We show in Figs. 4(a) and 4(b) the projection probabilities $\Pi_m(\theta)$ measured for an oversqueezed state [interaction time $t = 0.84(1)\tau$]. As theoretically shown in Ref. [40], we expect, for this protocol, optimal sensitivity around $\theta = 0$. We observe strong population variations

when the rotation axis $\hat{\mathbf{b}}$ coincides with the direction $\hat{\mathbf{n}}_{\max}$ of maximal spin projection variance [Fig. 4(b)] and minor variations for $\hat{\mathbf{b}} = \hat{\mathbf{n}}_{\min}$ [Fig. 4(a)]. To extract the metrological gain G, we calculate the Hellinger distances $d_{\mathrm{H}}^2(\theta, \theta')$ from the measured $\Pi_m(\theta)$ data and use a polynomial fit to extract its curvature around $\theta = \theta' = 0$ [45]. We show in Fig. 4(c) examples of cuts $d_{\mathrm{H}}^2(\theta, \theta' = 0)$, together with the corresponding fits. As shown in Fig. 4(d), we find that the measured gain agrees well for all rotation axes $\hat{\mathbf{b}}$ with the quantum Cramér-Rao bound for a pure state—the maximum achievable sensitivity—given by $2\Delta J_{\hat{\mathbf{b}}}^2/J$ [51]. The optimal character of this measurement protocol has been demonstrated theoretically in Ref. [40] and is based on the conservation of parity by the one-axis twisting Hamiltonian.

We repeat this measurement for various interaction times up to $t = 2\tau$ [see Fig. 4(e)]. For $t < 0.5\tau$, the measured gain G remains close to the usual gain $\bar{G}$ deduced from the first two moments, as expected in this regime of Gaussian quantum fluctuations [50]. For longer times, the measured gain G largely exceeds the gain $\bar{G}$, reaching an almost constant value $G = 8.6(6)$ in the oversqueezed regime (average value of $t > \tau$ data). This value is consistent with $G = J + 1/2$ expected for a spin state uniformly spanning the entire yz meridian. The measured sensitivity closely follows the one-axis twisting model prediction, and it remains close to the upper bound $(2/J)\Delta J_{\max}^2$ in the whole considered range of interaction times.

To get more physical insight we characterize the produced quantum states by their phase space representation on the generalized Bloch sphere. We consider in the following two quasiprobability distributions, the Wigner function W and the Husimi function Q [52,53]. The Wigner function, defined for a spin in [54], is an indicator of nonclassical behavior via its negative-value regions. The Husimi function $Q(\hat{\mathbf{n}})$, defined as the squared overlap with a coherent spin state pointing along $\hat{\mathbf{n}}$ [53], corresponds to a Gaussian smoothening of the Wigner function [55]. We compute both functions from the measured probabilities $\Pi_m(\hat{\mathbf{n}})$, using $Q(\hat{\mathbf{n}}) = \Pi_{m=J}(\hat{\mathbf{n}})$ and $W(\hat{\mathbf{n}}) = \sum_m (-1)^{J-m} a_m \Pi_m(\hat{\mathbf{n}})$, with $a_m \equiv \sum_{k=0}^{2J} (2k+1)\langle J, m, J, -m; k, 0\rangle/\sqrt{4\pi}$ [54]. As a reference, we measured the Husimi function of a coherent spin state [see Fig. 5(a)]. We find an almost isotropic Gaussian distribution of rms angular width $\delta\theta = 0.351(2)$, close to the expected value $1/\sqrt{J} \simeq 0.354$. For a short time $t = 0.48(2)\tau$, we reconstruct a twisted Husimi function, well described by an anisotropic Gaussian distribution [see Fig. 5(b)]. For $t = 2.2(1)\tau$, in the oversqueezed regime, the distribution has spread over the full yz meridian [see Fig. 5(c)]. Although semiclassical dynamics would predict diffusion toward a featureless distribution, we observe several small-scale dips that we interpret as the location of zeros of the Husimi function. For a pure quantum state $|\psi\rangle$ of a spin J,

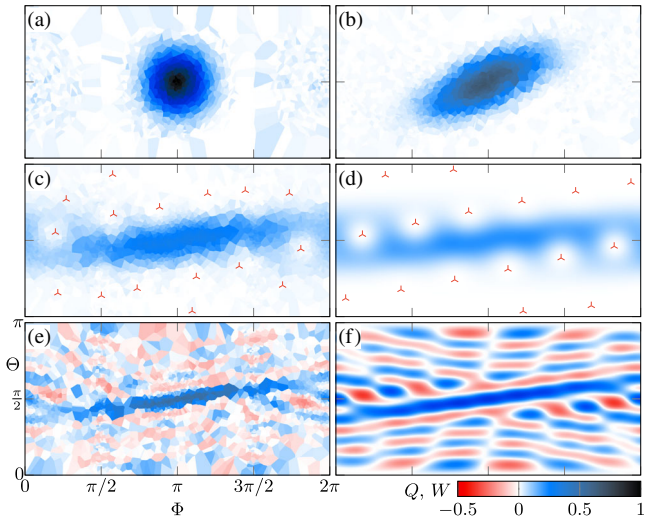

FIG. 5. (a)–(c) Husimi Q function measured for a coherent, squeezed, and oversqueezed spin states (a)–(c), achieved after evolution times $t/\tau = 0$, 0.48(2) and 2.2(1), respectively. The Bloch sphere is parametrized by the spherical angles (Θ, Φ) associated with the frame (y, z, x). The red stars in (c) indicate the fitted zeros of the Husimi function. (d),(f) Husimi (d) and Wigner (f) functions of the quantum state expected from the one-axis twisting model for an interaction time $t = 2.2\tau$. (e) Wigner function reconstructed from the same data used in (c).

we expect the occurrence of $2J$ zeros in the Husimi function, corresponding to the opposite orientations of the $2J$ fictitious spin-1/2 particles composing the spin J—the so-called Majorana stellar representation [56]. Denoting these orientations $\hat{\mathbf{u}}_i$ $(1 \leq i \leq 2J)$, the Husimi function reads $Q(\hat{\mathbf{n}}) \propto \prod_i (1 + \hat{\mathbf{u}}_i \cdot \hat{\mathbf{n}})$ and vanishes for $\hat{\mathbf{n}} = -\hat{\mathbf{u}}_i$ [57]. Fitting the entire distribution with this ansatz, we obtain the location of all zeros of the Husimi function, in good agreement with the expected positions [see Fig. 5(d)]. We show in Fig. 5(e) the Wigner function reconstructed for the oversqueezed state. It exhibits negative values in a large fraction of phase space, indicating a highly nonclassical character [58]. We also find small-scale oscillations reminiscent of "sub-Planck" structuring of phase space, as expected for metrologically useful quantum states [59]. Although the measured small-scale structures in the Husimi function are not directly linked to the magnetic sensitivity, the oscillations found in the Wigner function imply a fast variation of the state upon rotation, making a direct connection with the high magnetic sensitivity of oversqueezed states [60].

To conclude, we showed that measurements based on single magnetic sublevel resolution allow reaching optimal sensitivity with non-Gaussian states of a quantum spin J. An optimum $G = 8.6(6)$ is reached as soon as the spin distribution is stretched along the full yz meridian. The Heisenberg limit $G = 16$ could in principle be achieved using the maximally entangled N00N state [13,21]; however, the required interaction time $t = \sqrt{\pi^2 J/2}\tau$ is much

longer than τ for $J \gg 1$, making this state more fragile to decoherence [45]. Oversqueezed states thus appear as a compromise for future progress with large atomic ensembles. We also provided a full characterization of nonclassical spin states in phase space in terms of their Majorana stellar representation. The latter could be used to characterize ordering in spinor quantum gases [61], geometric quantum entanglement [62] or chaotic behavior [63].

We thank Chayma Bouazza for contributions in earlier stages of the experiment. This work is supported by PSL University (MAFAG project) and European Union (ERC UQUAM and TOPODY, Marie Curie project Grant No. 661433).

*Present address: LNE-SYRTE, Observatoire de Paris, Université PSL, CNRS, Sorbonne Université, 61 Avenue de l'Observatoire, 75014 Paris, France.
†sylvain.nascimbene@lkb.ens.fr

[1] C. W. Helstrom, J. Stat. Phys. **1**, 231 (1969).
[2] C. L. Degen, F. Reinhard, and P. Cappellaro, Rev. Mod. Phys. **89**, 035002 (2017).
[3] C. M. Caves, Phys. Rev. D **23**, 1693 (1981).
[4] D. J. Wineland, J. J. Bollinger, W. M. Itano, F. L. Moore, and D. J. Heinzen, Phys. Rev. A **46**, R6797 (1992).
[5] V. Giovannetti, S. Lloyd, and L. Maccone, Nat. Photonics **5**, 222 (2011).
[6] R. Demkowicz-Dobrzański, M. Jarzyna, and J. Kołodyński, in *Progress in Optics*, edited by E. Wolf (Elsevier, New York, 2015), Vol. 60, pp. 345–435.
[7] M. J. Holland and K. Burnett, Phys. Rev. Lett. **71**, 1355 (1993).
[8] B. L. Higgins, D. W. Berry, S. D. Bartlett, H. M. Wiseman, and G. J. Pryde, Nature (London) **450**, 393 (2007).
[9] J.-W. Pan, Z.-B. Chen, C.-Y. Lu, H. Weinfurter, A. Zeilinger, and M. Żukowski, Rev. Mod. Phys. **84**, 777 (2012).
[10] V. Meyer, M. A. Rowe, D. Kielpinski, C. A. Sackett, W. M. Itano, C. Monroe, and D. J. Wineland, Phys. Rev. Lett. **86**, 5870 (2001).
[11] D. Leibfried *et al.*, Nature (London) **438**, 639 (2005).
[12] C. F. Roos, M. Chwalla, K. Kim, M. Riebe, and R. Blatt, Nature (London) **443**, 316 (2006).
[13] T. Monz, P. Schindler, J. T. Barreiro, M. Chwalla, D. Nigg, W. A. Coish, M. Harlander, W. Hänsel, M. Hennrich, and R. Blatt, Phys. Rev. Lett. **106**, 130506 (2011).
[14] J. G. Bohnet, B. C. Sawyer, J. W. Britton, M. L. Wall, A. M. Rey, M. Foss-Feig, and J. J. Bollinger, Science **352**, 1297 (2016).
[15] A. Facon, E.-K. Dietsche, D. Grosso, S. Haroche, J.-M. Raimond, M. Brune, and S. Gleyzes, Nature (London) **535**, 262 (2016).
[16] A. Kuzmich, L. Mandel, and N. P. Bigelow, Phys. Rev. Lett. **85**, 1594 (2000).
[17] J. Appel, P. J. Windpassinger, D. Oblak, U. B. Hoff, N. Kjærgaard, and E. S. Polzik, Proc. Natl. Acad. Sci. U.S.A. **106**, 10960 (2009).
[18] I. D. Leroux, M. H. Schleier-Smith, and V. Vuletić, Phys. Rev. Lett. **104**, 073602 (2010).
[19] J. G. Bohnet, K. C. Cox, M. A. Norcia, J. M. Weiner, Z. Chen, and J. K. Thompson, Nat. Photonics **8**, 731 (2014).
[20] O. Hosten, N. J. Engelsen, R. Krishnakumar, and M. A. Kasevich, Nature (London) **529**, 505 (2016).
[21] T. Chalopin, C. Bouazza, A. Evrard, V. Makhalov, D. Dreon, J. Dalibard, L. A. Sidorenkov, and S. Nascimbene, Nat. Commun. **9**, 4955 (2018).
[22] A. Sørensen, L.-M. Duan, J. I. Cirac, and P. Zoller, Nature (London) **409**, 63 (2001).
[23] J. Estève, C. Gross, A. Weller, S. Giovanazzi, and M. K. Oberthaler, Nature (London) **455**, 1216 (2008).
[24] M. F. Riedel, P. Böhi, Y. Li, T. W. Hänsch, A. Sinatra, and P. Treutlein, Nature (London) **464**, 1170 (2010).
[25] J.-C. Jaskula, M. Bonneau, G. B. Partridge, V. Krachmalnicoff, P. Deuar, K. V. Kheruntsyan, A. Aspect, D. Boiron, and C. I. Westbrook, Phys. Rev. Lett. **105**, 190402 (2010).
[26] R. Bücker, J. Grond, S. Manz, T. Berrada, T. Betz, C. Koller, U. Hohenester, T. Schumm, A. Perrin, and J. Schmiedmayer, Nat. Phys. **7**, 608 (2011).
[27] E. M. Bookjans, C. D. Hamley, and M. S. Chapman, Phys. Rev. Lett. **107**, 210406 (2011).
[28] B. Lücke *et al.*, Science **334**, 773 (2011).
[29] C. D. Hamley, C. S. Gerving, T. M. Hoang, E. M. Bookjans, and M. S. Chapman, Nat. Phys. **8**, 305 (2012).
[30] H. Strobel, W. Muessel, D. Linnemann, T. Zibold, D. B. Hume, L. Pezzè, A. Smerzi, and M. K. Oberthaler, Science **345**, 424 (2014).
[31] X.-Y. Luo, Y.-Q. Zou, L.-N. Wu, Q. Liu, M.-F. Han, M. K. Tey, and L. You, Science **355**, 620 (2017).
[32] M. Kitagawa and M. Ueda, Phys. Rev. A **47**, 5138 (1993).
[33] L. Pezzè, A. Smerzi, M. K. Oberthaler, R. Schmied, and P. Treutlein, Rev. Mod. Phys. **90**, 035005 (2018).
[34] M. Gessner, A. Smerzi, and L. Pezzè, Phys. Rev. Lett. **122**, 090503 (2019).
[35] H. Zhang, R. McConnell, S. Ćuk, Q. Lin, M. H. Schleier-Smith, I. D. Leroux, and V. Vuletić, Phys. Rev. Lett. **109**, 133603 (2012).
[36] D. B. Hume, I. Stroescu, M. Joos, W. Muessel, H. Strobel, and M. K. Oberthaler, Phys. Rev. Lett. **111**, 253001 (2013).
[37] B. Yurke, S. L. McCall, and J. R. Klauder, Phys. Rev. A **33**, 4033 (1986).
[38] E. Davis, G. Bentsen, and M. Schleier-Smith, Phys. Rev. Lett. **116**, 053601 (2016).
[39] D. Linnemann, H. Strobel, W. Muessel, J. Schulz, R. J. Lewis-Swan, K. V. Kheruntsyan, and M. K. Oberthaler, Phys. Rev. Lett. **117**, 013001 (2016).
[40] S. P. Nolan, S. S. Szigeti, and S. A. Haine, Phys. Rev. Lett. **119**, 193601 (2017).
[41] L. D. Landau and E. Lifshitz, *Quantum Mechanics, Non-Relativistic Theory* (Pergamon Press, London, 1958).
[42] T. Chalopin *et al.*, Phys. Rev. A **98**, 040502(R) (2018).
[43] G. A. Smith, S. Chaudhury, A. Silberfarb, I. H. Deutsch, and P. S. Jessen, Phys. Rev. Lett. **93**, 163602 (2004).
[44] We estimate relative corrections to this coupling due to imperfect light polarization to remain below 0.05%. Furthermore, the laser detuning $\Delta = -2\pi \times 1.1(1)$ GHz ensures negligible incoherent Raman scattering over the typical light pulse duration $t \sim 100$ ns.

[45] See Supplemental Material at http://link.aps.org/supplemental/10.1103/PhysRevLett.122.173601 for details on the metrological gain in the presence of noise, experiment protocols, additional Hellinger distance data, Husimi and Wigner functions measured and computed for coherent and Gaussian squeezed states, and a discussion on the evaluation of purity of quantum states, which includes Refs. [46,47].
[46] G. M. D'Ariano, L. Maccone, and M. Paini, J. Opt. B **5**, 77 (2003).
[47] S. N. Filippov and V. I. Man'ko, J. Russ. Laser Res. **34**, 14 (2013).
[48] F. T. Arecchi, E. Courtens, R. Gilmore, and H. Thomas, Phys. Rev. A **6**, 2211 (1972).
[49] A. Holevo, in *Probabilistic and Statistical Aspects of Quantum Theory*, edited by A. Holevo, Publications of the Scuola Normale Superiore (Edizioni della Normale, Pisa, 2011), pp. 187–218.
[50] L. Pezzé and A. Smerzi, in *Atom Interferometry*, edited by G. M. Tino and M. A. Kasevich, Proceedings of the International School of Physics "Enrico Fermi"(IOS Press, Amsterdam, 2014), pp. 691–741.
[51] S. L. Braunstein and C. M. Caves, Phys. Rev. Lett. **72**, 3439 (1994).
[52] E. Wigner, Phys. Rev. **40**, 749 (1932).
[53] K. Husimi, J. Phys. Soc. Jpn. **22**, 264 (1940).
[54] J. P. Dowling, G. S. Agarwal, and W. P. Schleich, Phys. Rev. A **49**, 4101 (1994).
[55] M. Hillery, R. F. O'Connell, M. O. Scully, and E. P. Wigner, Phys. Rep. **106**, 121 (1984).
[56] E. Majorana, Nuovo Cimento **9**, 43 (1932).
[57] We also checked that the spin state remains quasipure on this timescale [45].
[58] A. Kenfack and K. Życzkowski, J. Opt. B **6**, 396 (2004).
[59] W. H. Zurek, Nature (London) **412**, 712 (2001).
[60] M. G. A. Paris, Int. J. Quantum. Inform. **07**, 125 (2009).
[61] D. M. Stamper-Kurn and M. Ueda, Rev. Mod. Phys. **85**, 1191 (2013).
[62] H. D. Liu and L. B. Fu, Phys. Rev. Lett. **113**, 240403 (2014).
[63] P. Leboeuf and A. Voros, J. Phys. A **23**, 1765 (1990).